Catalysis Today xxx (2014) xxx–xxx

Contents lists available at ScienceDirect

Catalysis Today

journal homepage: www.elsevier.com/locate/cattod

Photocatalytic and photoelectrocatalytic degradation of small biological compounds at TiO_2 photoanode: A case study of nucleotide bases

Guiying Li[a,b], Xiaolu Liu[a,b], Taicheng An[a,*], Hai Yang[a], Shanqing Zhang[b], Huijun Zhao[b,**]

[a] State Key Laboratory of Organic Geochemistry, Guangzhou Institute of Geochemistry, Chinese Academy of Sciences, Guangzhou 510640, China
[b] Centre for Clean Environment and Energy, Gold Coast Campus, Griffith University, Queensland 4222, Australia

ARTICLE INFO

Article history:
Received 9 January 2014
Received in revised form 18 April 2014
Accepted 21 April 2014
Available online xxx

Keywords:
Photocatalysis
Photoelectrocatalysis
Degradation
Nucleotide bases
Biological compounds

ABSTRACT

Photocatalytic (PC) and photoelectrocatalytic (PEC) degradation of small biological compounds such as nucleotide bases were carried out because of the nucleotide bases are the building blocks of large biomolecules, nucleic acids. These small biological compounds, four different nucleotide bases, can be photocatalytically and photoelectrocatalytically degradable, and the degradation efficiencies of PEC method were found to be higher than those of PC method for all compounds investigated. Also, we tried to propose the photocatalytical and photoelectrocatalytic degradation mechanisms of nucleotide bases, but the performance was unsuccessful. However, organic nitrogen in the original compounds was found to be oxidized to either NH_3/NH_4^+ or NO_3^- or both, depending on the chemical structures of the nucleotide bases and the degradation methods used. Based on both the experimental results and the theoretically calculated frontier electron densities (FED) values of $2FED_{HOMO}^2$ and $FED_{HOMO}^2 + FED_{LUMO}^2$, the conclusion can be demonstrated as the reaction mechanisms/pathways of PEC processes differed remarkably from that of PC processes.

1. Introduction

Photocatalytic (PC) degradation of a wide spectrum of organic compounds via TiO_2 photocatalysis has been well studied and documented [1–5]. Successful demonstration of the ability of illuminated TiO_2 for disinfection and decomposition of microorganisms has led to a new application field of TiO_2 photocatalysis [6–11]. Nevertheless, in strong contrast to the level of understanding toward the degradation of organic compounds, little has been known regarding the mechanistic steps of PC degradation of microbial cells at the molecular level [12–16]. It is well known that a microbial cell is built by different classes of large biomolecules (e.g., lipid, protein and DNA/RNA). These large biomolecules consist of large numbers of basic building blocks (e.g., fatty acids, amino acids and nucleotide bases). A conjectural view of microbial cell degradation is that the process is highly complex as it involves the initial breaking down of the microbial cell into large biomolecules then to basic building blocks before the mineralization can be achieved. A sensible approach to investigate such complex processes would therefore be a bottom-up approach to investigate and understand the degradation behaviors of basic building blocks such as nucleotide bases.

Pyrimidine and purine are two essential classes of the nucleotide bases. They exist not only in natural biological species (e.g., DNA, RNA and enzyme cofactors) but also as pollutants in environment resulted from the degradation of biological species, agrochemicals (i.e., insecticides) and medicines (i.e., antibiotics) [17–20]. PC degradation of nucleotide bases has been reported by a number of research groups [12,14,17,21,22]. Hidaka et al. [12] investigated the fate of DNA and RNA under UVA and UVB irradiation in the presence of TiO_2 by examining degradation products of the pyrimidine and purine. CO_2, NH_3 and NO_3^- were produced under the illumination. Horikoshi et al. [14] employed UV–vis spectroscopy and gas chromatography together with calculated point of charges and frontier electron densities (FEDs) to assess the effect of the chemical structures of the nucleotide bases on their photocatalytic mineralization behavior. Dhananjeyan et al. [21] reported the rate of PC degradation of uracil (U), thymine (T) and 6-methyluracil in TiO_2 aqueous suspension can be expressed by Langmuir–Hinshelwood equation. Singh et al. [17] and Bahnemann et al. [22] investigated PC degradation of U and other organics under a variety of

* Corresponding author. Tel.: +86 20 85291501; fax: +86 20 85290706.
** Corresponding author. Tel.: +61 7 555 2 8261; fax: +61 7 5552 8067.
E-mail addresses: antc99@gig.ac.cn (T. An), h.zhao@griffith.edu.au (H. Zhao).

http://dx.doi.org/10.1016/j.cattod.2014.04.029
0920-5861/

conditions and claimed that P25 was more efficient than other forms of TiO_2 photocatalysts investigated.

Nucleotide bases are nitrogen containing compounds. Thus the degradation extent of original compounds can be strongly influenced by the mineralization products of organic nitrogen [23,24] although a number of investigations have been carried out to examine the mineralization products of organic nitrogen [23–26]. Together with various other intermediates, the ultimate mineralization products of such compounds are usually expected to lead to the formation of N_2 gas, NH_3 and/or NO_3^- through photocatalytic oxidative pathways [26]. The formation of these products was closely related to the chemical structure of the initial substrates. Nitro groups are converted predominantly to NO_3^- through NO_2^- intermediate [27], while the amine group was almost always converted to NH_4^+, whereas the amount of NO_3^- produced was nearly negligible, although a slow transformation of NH_4^+ into NO_3^- is observed at longer irradiation times. It was also reported that hydroxylated amines tended to be converted into NO_3^- while the amide group favorably transformed into NH_4^+ at rates faster than that of amine groups [23,28]. The heterorings containing an N=N fragment would normally lead to the evolution of N_2 but for those containing a C—N=C fragment, the NH_4^+ was obtained as the main product [24]. Furthermore, mechanistic aspects of nucleotide bases have been tentatively investigated [18,29,30]. Cathcart et al. [29] reported that base glycols is an important class of DNA degradation intermediates, and Dhananjeyan et al. [30] reported the thymine glycol was produced during PC degradation of T. Jaussaud et al.'s [18] reported that during PC degradation of U, the first step of the mineralization could lead to the formation of uracil glycol, and then followed by the further oxidation of uracil glycol to polyol, carboxylic and aldehyde.

Also, the high degradation efficiency of photoelectrocatalysis toward broad spectrum organic compounds has been widely acknowledged [1,2,31]. The applied potential bias to timely remove the photogenerated electrons and physical separation of photoanode from the cathode are generally regarded as the main attributes for the enhanced efficiency [32–34]. It has also been recognized that the applied potential bias also prolongs the lifetime of photoholes, enabling direct photohole reactions [1,33], thus enhances the degradation efficiency as the oxidation power of the photoholes (3.1 V) is greater than that of photogenerated radicals such •OH [35]. More importantly, the mechanistic pathway of a photoelectrocatalytic (PEC) degradation process may differ from that of PC degradation process because of the differences when h^+ and •OH act as oxidants. Despite numerous studies on PEC degradation of organics have been previously reported [1,2,34,36,37], the PEC degradation of nucleotide bases has not been studied yet.

In this study, PC and PEC degradation of nucleotide bases at an illuminated nanoparticulate TiO_2 photoanode were systematically investigated using a thin-layer photoelectrochemical cell. All experiments were carried out under comparable experimental conditions, enabling a meaningful comparison of PC and PEC degradation processes. Four different nucleotide bases, U, T, cytosine (C) and adenine (A) were used as test compounds to represent pyrimidine and purine bases. Degradation efficiencies of all test bases for both PC and PEC processes were examined. For a given base, the mineralization ratios of PEC/PC processes were quantified, and a PLC system equipped with a PDA detector was employed to obtain the information of PC and PEC degradation products. The FEDs of all test bases were calculated, and the calculated $2FED_{HOMO}{}^2$ and $FED_{HOMO}{}^2 + FED_{LUMO}{}^2$ values [38,39], and the degradation product information obtained from the chromatograms were collectively utilized to illustrate the mechanistic aspects of PC and PEC degradation processes.

2. Materials and methods

2.1. Materials

The substrates examined were four nucleotide bases including U, T, C and A, as well as titanium butoxide, acetonitrile and sodium perchlorate were supplied by Sigma. Indium tin oxide conducting glass slides (ITO, 8 Ω/square) were purchased from Delta Technologies Ltd. (USA). All solutions were prepared using high purity deionized water (Millipore Corp., 18 MΩ cm).

2.2. Apparatus and methods

Both PC and PEC degradation experiments were performed under identical UV intensity using the same UV–LED array/TiO_2 photoelectrochemical cell [40,41]. That is, the cell consists of a TiO_2 photoanode as the working electrode, a Ag/AgCl reference electrode and a Pt disk auxiliary electrode. The TiO_2 photoanode was prepared by hydrolysis of titanium butoxide according to our previously described method [42], which was consisted of 96.6% anatase and 3.4% rutile. The resultant TiO_2 photoanode was very stabile and only 1 piece of photoanode is used for all of the experiment in this work. The thickness of the reaction chamber and the illumination area were 0.25 mm and 462 mm^2, respectively. A UV–LED array consisted of 4 pieces of UV–LED (NCCU033(T), Nichia Corporation) was used as the illumination source. The specified peak wavelength of the LED was 365 nm with a spectrum half width of 8 nm. For PEC degradation experiments, a 2.0 M $NaNO_3$ solution was used as the supporting electrolyte. A voltammograph (cv-27, BAS) was used for electrochemical control. Potential and current signals were monitored using a computer coupled with a Maclab 400 interface (AD Instruments). For the exhaustive degradation experiment, a sample containing various concentrations of nucleotide bases and 2.0 M $NaNO_3$ was injected into the thin-layer cell via a precision pump before the degradation process and then subjected to PC and PEC oxidation. For samples need HPLC analysis after PC and PEC oxidation, a continuous sample injection model via a precision pump during the degradation process was used. Under such conditions, the reaction time of a sample was controlled by adjusting the flow rate. A sufficient volume of the reacted sample was collected for further analyses after the system reaching its steady-state for which the collected sample had been subjected to the same reaction time. A 2.0 M $NaNO_3$ solution was used to clean the cell in between the two sample injections. PC degradation experiments were conducted under identical experimental conditions as PEC experiments, except the electrochemical system was disconnected.

2.3. Analysis

For PC and PEC experiments, the extent of the mineralization was determined by measuring the charge originated from the oxidation of nucleotide bases using PeCOD™ technique [34,42], and the detailed calculation produce is the same as our previous work [3].

Intermediate degradation products were analyzed using a Waters 996 HPLC/MS (Micromass, Manchester, UK) equipped with a PDA detector and an electro-spray ionization (ESI) source. The elution was carried out using a Gemini-NX C18 column (Phenomenex, USA). The separation of nucleotide bases and the intermediates was performed with isocratic elution using a 95%/5% by volume eluent A and eluent B mixture. Eluent A is 600 μM ammonium acetate solution. Eluent B is HPLC grade acetonitrile. The eluent flow rate was maintained throughout at 1 ml/min. Nitrogen was used as nebulizer and dry gas. The PDA detection wavelength was set between 191 and 400 nm for acquiring chromatograms and quantitative analysis. The mass spectrum was obtained from 50 to 300 *m*/*z*. The mass

Please cite this article in press as: G. Li, et al., Photocatalytic and photoelectrocatalytic degradation of small biological compounds at TiO_2 photoanode: A case study of nucleotide bases, Catal. Today (2014), http://dx.doi.org/10.1016/j.cattod.2014.04.029

spectrometer was operated in positive ion mode. The cone voltage is 30 V for each of the sample.

2.4. Frontier electron densities calculations

The molecular orbital calculations were carried out by using Gaussian 03 program (Gaussian, Inc.) at the single determinant level (HF/3-21) with the optimal conformation having minimum energy obtained at the B3LYP/6-31G* level. And then the FEDs of the highest occupied molecular orbital (HOMO) and the lowest unoccupied molecular orbital (LUMO) were calculated. The obtained values of $2FED_{HOMO}^2$ and $FED_{HOMO}^2 + FED_{LUMO}^2$ were used to predict the reaction sites for electron extraction and radical attack, respectively [38,39].

3. Results and discussion

3.1. Photocatalytic degradation

The nucleotide bases contain organic nitrogens that can be mineralized to different oxidation states (i.e., HN_3/NH_4^+ and NO_3^-). It has been reported that for photocatalytic degradation of formamide and urea, the mineralization products of organic nitrogen are largely depended on the oxidation state of C atom to which the N heteroatom is bonded, rather than on the oxidation state of N [26,43]. The C bonding to N in urea has a formal oxidation state of +4 and presents no extractable bonded H to that carbon. In this case, •OH is likely to attack at —NH_2 group, leading to formation of NO_3^- as main product [23]. In contrast, when the bonded C to N is in a lower oxidation state, as found in formamide that has a formal oxidation state of +2 and with extractable H atoms, evolution of NH_3/NH_4^+ is favored [23]. However, the conversion ratios of NH_4^+/NO_3^- are varied depending on the type of organics and experimental conditions [23]. Hence, precisely assigning the measured charge transfer to mineralization products with organic nitrogens being converted to NH_3/NH_4^+ or NO_3^- is difficult. Table 1 summaries the number of electron transfer required for mineralizing organic nitrogens of different bases to NH_3/NH_4^+ (n_{NH_3/HN_4^+}) and NO_3^- ($n_{NO_3^-}$). It is obvious that the extent of mineralization will be strongly influenced by final mineralization products of the organic nitrogens. For this work, the mineralization percentages were calculated by assigning the measured charge transfer to mineralization products with organic nitrogens being 100% converted to NH_3/NH_4^+ or NO_3^-.

Fig. S1 shows a set of typical photocurrent–time profiles obtained from U samples before and after PC treatment. These photocurrent profiles are used to obtain the percentage mineralization of PC treated samples by measuring the amount of electrons lost during the PC treatment [3]. Fig. 1 shows the plots of the mineralization percentage of PC treated samples against the equivalent electron concentration (C_{eq}) for organic nitrogens mineralized to NH_3/NH_4^+ and NO_3^-. All samples were photocatalytically treated for 300 s under a UV intensity of 8.0 mW/cm^2. The equivalent electron concentrations were calculated according to $C_{eq} = n_{NH_3/HN_4^+} \cdot C_M$ for Fig. 1a and $C_{eq} = n_{NO_3^-} \cdot C_M$ for Fig. 1b,

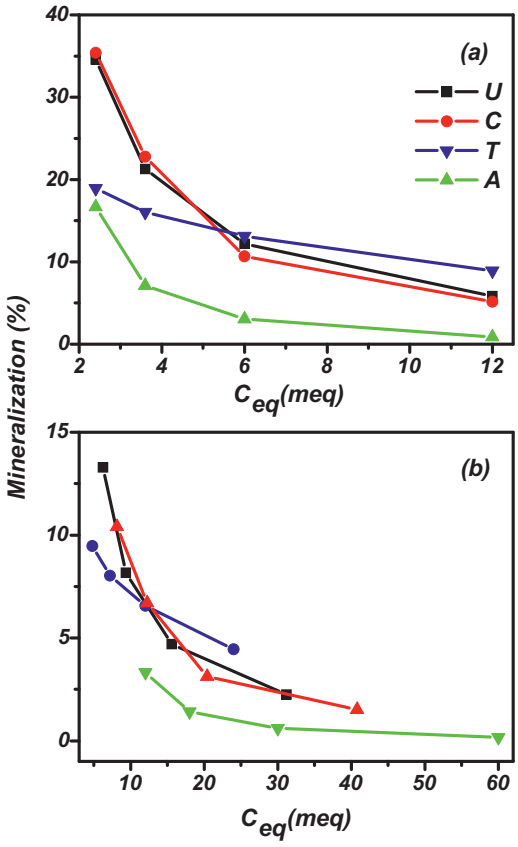

Fig. 1. Photocatalytic degradation of uracil (U), cytosine (C), thymine (T) and adenine (A): (a) mineralization percentage against C_{eq} for N oxidized to NH_3 and (b) to NO_3^-.

respectively, where C_M is the molar concentration of bases. The use of C_{eq} allows a more meaningful comparison among different bases because such a non-characteristic concentration unit represents the electron demands for complete mineralization [2]. More importantly, the electron demand for a given C_{eq} is the same for all bases, regardless of their chemical structures and electron transfer numbers [2]. For all cases investigated, an increase in C_{eq} led to a decrease in the mineralization percentage for conversion to both NH_3/NH_4^+ and NO_3^-. Except for T, rapidly decreased mineralization percentage with increased C_{eq} within low concentration rage for all other PC treated bases was observed. In cases of conversion to both NH_3/NH_4^+ and NO_3^-, T also exhibited a lower mineralization percentages at lower concentrations but higher mineralization percentage at higher concentrations than the other two pyrimidine bases. The mineralization percentage values and the effect of C_{eq} on these values for the other two pyrimidine bases were very similar. It was also observed that the mineralization percentages of single-ringed pyrimidine bases (i.e., U, C and T) within the concentration range investigated were higher than that of double-ringed purine bases (i.e., A).

Table 1
Number of electrons required for complete mineralization of N to NH_3/NH_4^+ (n_{NH_3/HN_4^+}) and NO_3^- ($n_{NO_3^-}$).

Nucleotide bases	n_{NH_3/HN_4^+}	$n_{NO_3^-}$	$n_{NH_3/HN_4^+}/n_{NO_3^-}$
Uracil ($C_4H_4N_2O_2$)	10	26	0.385
Thymine ($C_5H_6N_2O_2$)	16	32	0.500
Cytosine ($C_4H_5N_3O$)	10	34	0.294
Adenine ($C_5H_5N_5$)	10	50	0.200

3.2. Photoelectrocatalytic degradation

All samples were photoelectrocatalytically treated under the identical experimental conditions to PC experiments except with an applied potential bias of +0.30 V vs. Ag/AgCl. Fig. S2 shows a set of typical photocurrent–time profiles obtained from T samples during PEC treatment. These photocurrent profiles are used to obtain the percentage mineralization of PEC treated samples by measuring the amount of electrons lost during the PEC treatment in accordance with equation, mineralization (%) = $Q_{net}/Q_{th} \times 100\%$.

Please cite this article in press as: G. Li, et al., Photocatalytic and photoelectrocatalytic degradation of small biological compounds at TiO_2 photoanode: A case study of nucleotide bases, Catal. Today (2014), http://dx.doi.org/10.1016/j.cattod.2014.04.029

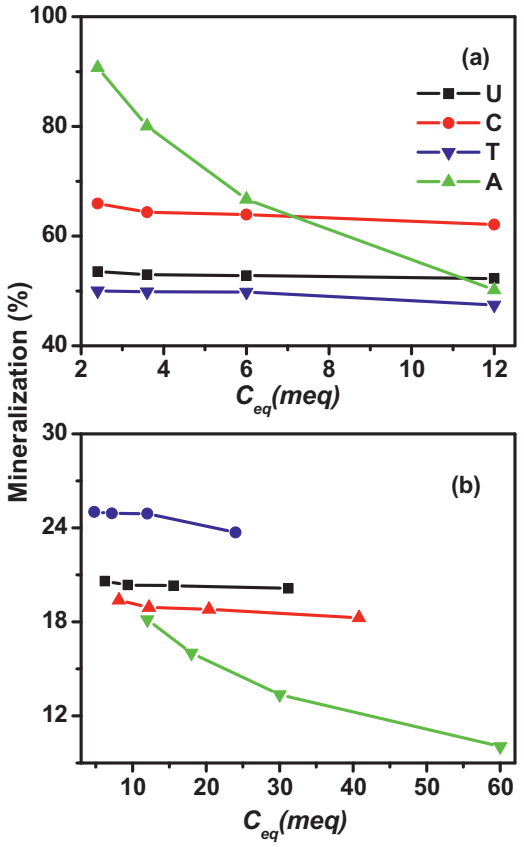

Fig. 2. Photoelectrocatalytic degradation of uracil (U), cytosine (C), thymine (T) and adenine (A): (a) mineralization percentage against C_{eq} for N oxidized to NH_3 and (b) to NO_3^-.

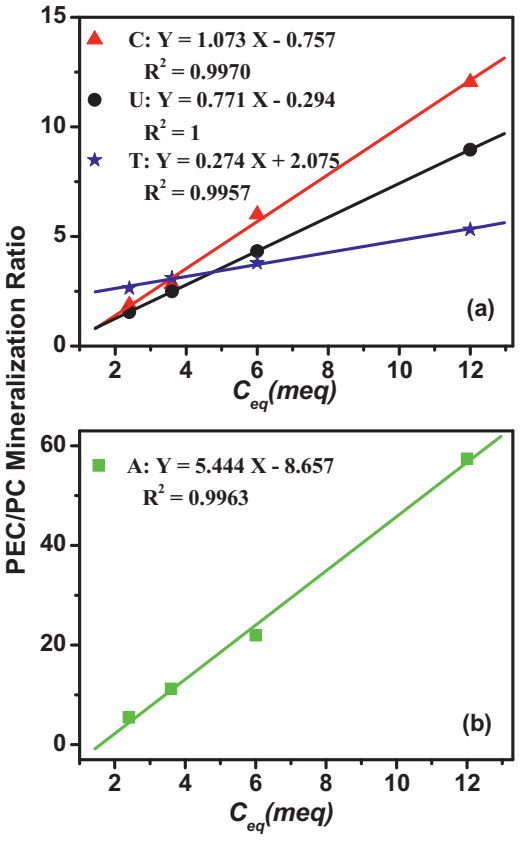

Fig. 3. A plot of PEC to PC mineralization ratio against C_{eq} for (a) uracil (U), cytosine (C), and thymine (T) and (b) adenine (A).

Fig. 2 shows the plots of the mineralization percentage of PEC treated nucleotide bases samples against C_{eq} for organic nitrogens mineralized to NH_3/NH_4^+ and NO_3^-. In strong contrast to the PC treated samples, the effect of concentration of pyrimidine on the mineralization percentage was insignificant, while for purine like A, the mineralization percentage decreased as C_{eq} was increased. The extent of mineralization of PEC treated samples was much higher than that of PC, suggesting a higher PEC degradation efficiency. For A converting to NH_3/NH_4^+ within lower concentration range (i.e., C_{eq} < 6 meq of electrons), the mineralization percentages were higher than that of all pyrimidine investigated (Fig. 2a). The mineralization percentages of A to NH_3/NH_4^+ were higher than that of T within whole concentration range investigated. For converting to $NH_3/NH_4^+NO_3^-$, the mineralization percentages within lower concentration range followed A > C > U > T (Fig. 2a). However, a completely reversed order of T > U > C > A within the entire concentration range was observed for converting to NO_3^- (Fig. 2b). Interestingly, the electron transfer number ratio ($n_{NH_3/HN_4^+}/n_{NO_3^-}$) followed an order of T > U > C > A, which is in the same as the order of the mineralization percentages for converting to NO_3^- but reversed for converting to NH_3/NH_4^+ (Table 1). This suggests that carbon to nitrogen ratio and their oxidation states in original bases determines the extent of mineralization under PEC conditions. These characteristics are distinctively different to those observed from PC treated samples.

The differences between PEC and PC in respect to the extent of mineralization were quantitatively evaluated by plotting the PEC/PC ratio against C_{eq} (Fig. 3). Surprisingly, linear relationships were obtained for all cases investigated. Such liner relationships reveal that the superiority (in terms of mineralization efficiency) of PEC method over PC method increases as concentration increases. Furthermore, the slope of curve quantifies the superiority degree of PEC method over PC method in respect to the concentration change. The obtained slops were found to follow an order of A(5.44 meq^{-1}) > C(1.07 meq^{-1}) > U(0.77 meq^{-1}) > T(0.27 meq^{-1}), which is the reversed order of $n_{NH_3/HN_4^+}/n_{NO_3^-}$ (Table 1). This again suggests that carbon to nitrogen ratio and their oxidation states in the original bases determines PEC/PC mineralization efficiency ratio. These also suggest that the characteristics of a PEC degradation process differ markedly from a PC degradation process. Such differences could be due to the reaction pathway differences between the two processes that deserve a further investigation.

3.3. Photocatalytic and photoelectrocatalytic degradation products

From the experimental results obtained above, it is clearly demonstrated the degradation behavior of the nucleotide bases differences between PC and PEC processes, which could be due to the mechanistic pathway differences between two processes. Theoretically calculated FEDs have been recognized as a useful tool for predicting initial reaction sites for direct h^+ and $^\bullet OH$ attack by the obtained values of $2FED_{HOMO}^2$ and $FED_{HOMO}^2 + FED_{LUMO}^2$, respectively [38,39]. As known, direct h^+ attack is likely to occur in a PEC degradation process than that of a PC process. This could be one of the most important attributes that deviates the mechanistic pathways of PEC from PC process.

The values of $2FED_{HOMO}^2$ and $FED_{HOMO}^2 + FED_{LUMO}^2$ were therefore calculated and used to evaluate the initial reaction steps of PC and PEC processes (Table 2). For U, higher $2FED_{HOMO}^2$ values were obtained for C^5 (0.5034) and N^3 (0.4190) indicating the initial h^+ attacks are likely to occur on a double-bonded carbon atom and a

Please cite this article in press as: G. Li, et al., Photocatalytic and photoelectrocatalytic degradation of small biological compounds at TiO_2 photoanode: A case study of nucleotide bases, Catal. Today (2014), http://dx.doi.org/10.1016/j.cattod.2014.04.029

Table 2
Frontier electron densities (FEDs) on atoms of nucleotide bases calculated by using Gaussian 03 Program.

Uracil

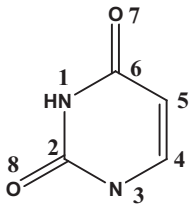

Atom	$2FED_{HOMO}^2$	$FED_{HOMO}^2 + FED_{LUMO}^2$	Atom	$2FED_{HOMO}^2$	$FED_{HOMO}^2 + FED_{LUMO}^2$
N^1	0.0000	0.0630	C^5	0.5128	0.2827
C^2	0.0006	0.0038	C^6	0.0050	0.1473
N^3	0.4190	0.3333	O^7	0.0163	0.2169
C^4	0.1610	0.5053	O^8	0.1120	0.0917

Cytosine

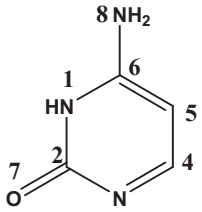

Atom	$2FED_{HOMO}^2$	$FED_{HOMO}^2 + FED_{LUMO}^2$	Atom	$2FED_{HOMO}^2$	$FED_{HOMO}^2 + FED_{LUMO}^2$
N^1	0.3018	0.3355	C^5	0.3588	0.1815
C^2	0.0006	0.0460	C^6	0.0126	0.1750
N^3	0.2425	0.3034	O^7	0.1882	0.2349
C^4	0.0848	0.5945	N^8	0.0108	0.0791

Thymine

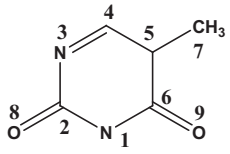

Atom	$2FED_{HOMO}^2$	$FED_{HOMO}^2 + FED_{LUMO}^2$	Atom	$2FED_{HOMO}^2$	$FED_{HOMO}^2 + FED_{LUMO}^2$
N^1	0.0006	0.0857	C^6	0.0024	0.1649
C^2	0.0010	0.0309	C^7	0.0342	0.1069
N^3	0.3932	0.2490	O^8	0.1142	0.1141
C^4	0.1960	0.4955	O^9	0.1220	0.1966
C^5	0.5034	0.3643			

Adenine

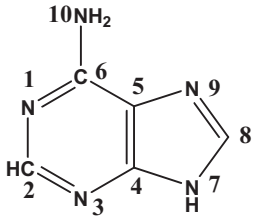

Atom	$2FED_{HOMO}^2$	$FED_{HOMO}^2 + FED_{LUMO}^2$	Atom	$2FED_{HOMO}^2$	$FED_{HOMO}^2 + FED_{LUMO}^2$
N^1	0.0422	0.0424	C^6	0.0804	0.2691
C^2	0.0996	0.1923	N^7	0.0304	0.0831
N^3	0.2142	0.2256	C^8	0.1980	0.3050
C^4	0.0728	0.0192	N^9	0.1300	0.1117
C^5	0.2484	0.1209	N^{10}	0.2990	0.2816

nitrogen atom that is connected to a carbon atoms with —C=C— and >C=O bonds. For •OH attacks, the obtained $FED_{HOMO}^2 + FED_{LUMO}^2$ values indicate C^4 (0.5053) and N^3 (0.3333) are likely to be the initial reaction sites. C^4 is also a double-bonded carbon atom but located on the other end of double bond. Similar results were obtained from C where higher probability for h^+ (C^5, 0.3588) and •OH (C^4, 0.5945) to attack carbon atoms at different ends of —C=C— but on the same nitrogen atom (N^1, 0.3018 for h^+ and 0.3355 for •OH). For T, the highest probability of initial reaction sites for h^+ (C^5, 0.5034) and •OH (C^4, 0.4955) induced reactions were also similar to the other two pyrimidine. A slight difference is that •OH may also attack the same carbon atom (C^5) as h^+ does. For A, the calculated $2FED_{HOMO}^2$ values suggest that the initial h^+ induced reaction site is more likely to occur at a side-chain nitrogen atom (N^{10},

Please cite this article in press as: G. Li, et al., Photocatalytic and photoelectrocatalytic degradation of small biological compounds at TiO_2 photoanode: A case study of nucleotide bases, Catal. Today (2014), http://dx.doi.org/10.1016/j.cattod.2014.04.029

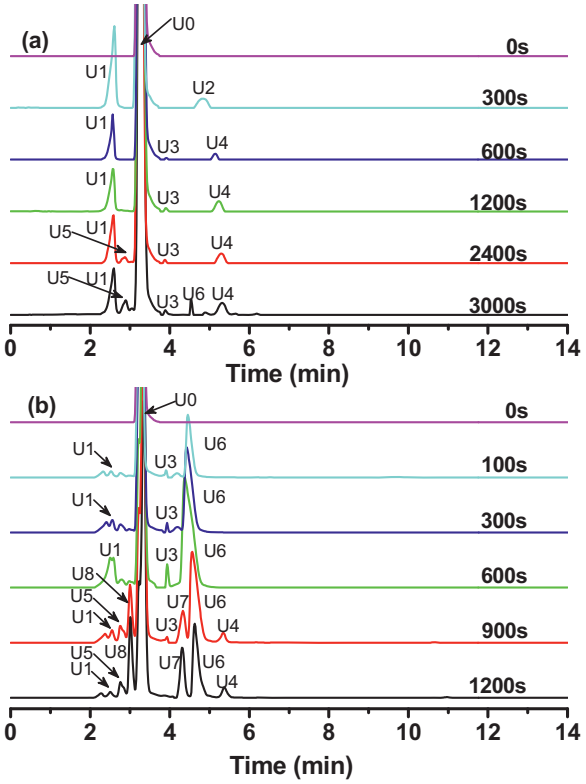

Fig. 4. The chromatograms obtained for PC (a) and PEC (b) treated uracil samples at different reaction intervals under 8.0 mW/cm^2 UV intensity. Initial concentration: 12 meq (N oxidized to NH_3); applied potential bias for PEC: +0.40 V vs. Ag/AgCl; retention time: t_R(U0) = 3.2 min; t_R(U1) = 2.5 min; t_R(U2) = 4.8 min; t_R(U3) = 3.9 min; t_R(U4) = 5.4 min; t_R(U5) = 2.7 min; t_R(U6) = 4.5 min; t_R(U7) = 4.3 min; t_R(U8) = 3.0 min.

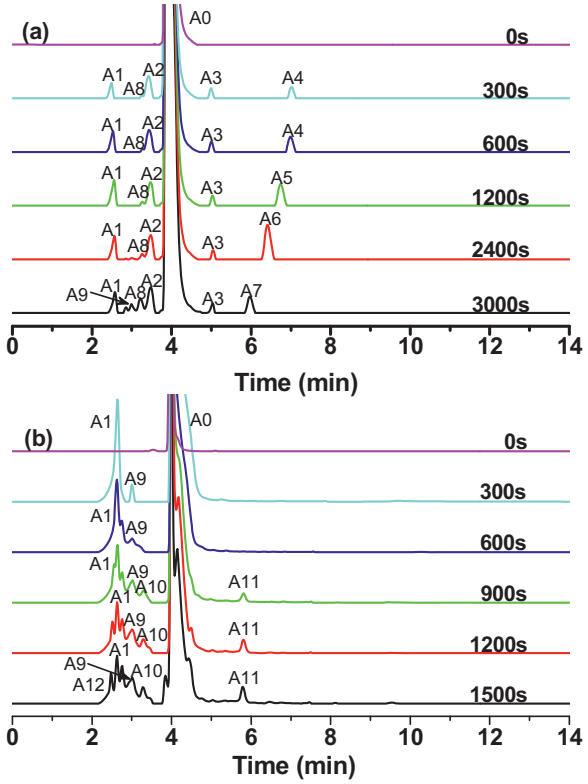

Fig. 5. The chromatograms obtained for PC (a) and PEC (b) treated adenine samples at different reaction intervals under 8.0 mW/cm^2 UV intensity. Initial concentration: 12 meq (N oxidized to NH_3); applied potential bias for PEC: +0.40 V vs. Ag/AgCl; retention time: t_R(A0) = 4.0 min; t_R(A1) = 2.6 min; t_R(A2) = 3.4 min; t_R(A3) = 5.9 min; t_R(A4) = 7.0 min; t_R(A5) = 6.7 min; t_R(A6) = 6.4 min; t_R(A7) = 6.0 min; t_R(A8) = 3.2 min; t_R(A9) = 3.9 min; t_R(A10) = 3.3 min; t_R(A11) = 5.8 min; t_R(A12) = 2.5 min.

0.2990) rather than on carbon atoms within the 6-membered ring structure as pyrimidine. For •OH induced initial reaction site, the C^8 (0.3050) located within 5-membered ring structure would be the most favorable initial reaction site. A summary of the above observations is that the predicted favorable initial reaction sites induced by h^+ and •OH are different for all cases investigated. This may mean a mechanistic pathway difference for PC and PEC processes.

The calculated FEDs results suggested that PC and PEC might undergo different mechanistic pathways because of the initial reaction site differences when a given nucleotide base was attacked by h^+ and •OH. If these FEDs predictions are true, then different intermediates should be obtained from PC and PEC treated samples. Experiments were therefore carried out to determine intermediates of PC and PEC treated samples (Figs. 4, S3, S4 and 5). It should be noted that although the Waters 996 HPLC/MS was equipped with both PDA and ESI detectors, the attempt to directly identify the intermediates based on ESI response failed due to the high noisy to signal ratio.

Fig. 4a shows the chromatograms of PC treated U samples. For samples without treatment, an absorption peak (U0) with a retention time (t_R) of 3.2 min, signifying the original U molecule was observed. After 300 s treatment, U1 (t_R = 2.5 min) and U2 (t_R = 4.8 min) were detected as earlier degradation intermediates. U1 was more hydrophilic than that of uracil. After 600 s treatment, U1 concentration decreased to approximately half as in 300 s PC treated sample, while U2 decreased to below the detection limit. Two new intermediates (U3 and U4) more hydrophobic than U were detected at t_R = 3.9 and 5.4 min, respectively. With further increase of treatment time, U1 remains as a dominant intermediate but its concentration was unchanged. An additional intermediate (U5) more hydrophilic than U was detected after 2400 s treatment and its concentration increased with treatment time. For U3 and U4, their concentrations slightly increased with further increase of treatment time. A new intermediate (U6) more hydrophobic than U was detected after 3000 s treatment. The intermediates more hydrophilic than U (U1 and U5) could be uracil glycols [18] as a result of •OH attack on C^4 (Table 2). However, the formation of intermediates (U2, U3, U4 and U6) more hydrophobic than uracil is difficult to explain because all published •OH attack mechanisms are exclusively led to the formation of more hydrophilic glycols [18,38,39]. The formation of more hydrophobic intermediates may imply the deficiencies of existing mechanisms.

Fig. 4b shows the chromatograms of PEC treated U samples. An identical chromatogram was observed from the samples without treatment. Comparatively, except U2, all intermediates detected from PC treated samples were also detected from PEC treated samples. In addition, two new intermediates (U7 and U8) were also detected. Specifically, these chromatograms revealed a number of noticeable differences between photocatalysis and photoelectrocatalysis. The concentration of U1 was much lower than that of PC treatment, suggesting U1 is not a dominant intermediate in PEC process. Instead, a new intermediate (U8) became the dominant hydrophilic intermediate for PEC treated samples greater than 900 s. U3 concentration increased with reaction time up to 600 s and then decreased to below the detection limit at 1200 s. U4 concentrations were similar to PC treated samples but can be detected with treatment greater than 900 s. U6 could only be detected with PC 3000 s or longer treatment, whereas it was a prime intermediate with much higher concentration for PEC treatment. Its concentration increased with treatment time up to 600 s but decreased

Please cite this article in press as: G. Li, et al., Photocatalytic and photoelectrocatalytic degradation of small biological compounds at TiO_2 photoanode: A case study of nucleotide bases, Catal. Today (2014), http://dx.doi.org/10.1016/j.cattod.2014.04.029

slightly due to the formation of a new intermediate (U7). In fact, the two hydrophobic intermediates (U6 and U7) were the dominant PEC degradation products in the reaction mixtures.

Fig. S3 shows the chromatograms of PC and PEC treated C samples. The original cytosine absorption peak (C0) was observed at t_R = 3.0 min. For PC treatment (Fig. S3a), a dominant intermediate adsorption peak (C1, t_R = 2.8 min), more hydrophilic than C, was recorded, and its concentration increased as the treatment time increased. Additionally, three intermediates (C2, C3 and C4) more hydrophobic than C with retention times of 3.3, 3.8 and 4.0 min, respectively, were observed. Their concentrations were much lower than that of C1.

For PEC treatment (Fig. S3b), C1 becomes a minor intermediate in comparison to PC treated samples. The intermediates of C2, C3 and C4 were all recorded as minor intermediates. The samples subjected to PEC treatment equal to or greater than 600 s, the concentration of C2 was slightly higher that that of PC treated samples. Compared with PC treated samples, two additional minor intermediates (C5 and C6) more hydrophilic than that of C were recorded at t_R = 2.4 and 2.6 min, respectively. However, seven additional intermediates (C7–C13) more hydrophobic than C were observed. C7 (t_R = 4.5 min) was the dominant intermediate for the 100 s PEC treatment sample but its concentration rapidly deceased as the treatment time up to 900 s. C8 (t_R = 5.0 min) concentration decreased when the treatment time increased from 100 to 300 s, but rapidly increased when treatment time was greater than 600 s. It became one of the dominant intermediates for PEC 900 s or longer treated samples. The intermediate C9 (t_R = 4.8 min) was observed from samples with PEC treatment times equal to or greater than 300 s. Its concentration was increased as the treatment time increased. C9 was the dominant intermediate for 300 s PEC treated sample and remain when the treatment time was further increased. It should be noted that C0 concentration rapidly decreased as C9 forming and reduced to below detection limit when C9 and C8 co-dominated at PEC 1200 s. The intermediates of C10–C12 were minor intermediates with low concentrations. Interestingly, a very hydrophobic intermediate (C13, t_R = 13.6 min) was observed from samples treated for 600 s or longer. Its concentration increased with treatment time and continued to increase even after C was completely decomposed, suggesting that C13 was produced from the further oxidation of intermediates.

Fig. S4 shows the chromatograms of PC and PEC treated T samples. The absorption peak (T0) observed at t_R = 4.4 min can be assigned to the original T. For PC treatment (Fig. S4a), intermediates T1 and T2 both are more hydrophilic than T, were detected at t_R = 3.1 and 3.7 min, respectively. Their concentrations increased with the increase of reaction time. Interestingly, no other detectable intermediates were recorded for PC treated samples. For PEC treatment (Fig. S4b), T (T0) was completely consumed after PEC 300 s treatment. T1 became a minor intermediate in comparison to PC treated samples, while T2 was not observed. A group of intermediates (T4, T5, T7 and T8) more hydrophilic than T were recorded as minor intermediates. More hydrophobic intermediates (T3, T6 and T9) were also detected. T3 appeared as a dominant intermediate in 100 s PEC treated sample and rapidly decreased to below the detection level after 600 s. T6 was the dominate intermediate for samples treated for 100 s or longer. Its concentration increased with the increase of treatment time, even after T was reduced to below the detection limit, indicating that T6 was a further oxidation product of intermediates rather than the direct oxidation product of T. T9 was one of the major hydrophobic intermediate for PEC treated samples with treatment time equal to or greater than 300 s.

Fig. 5 shows the chromatograms of PC and PEC treated A samples. The absorption peak of A (A0) was observed at t_R = 4.0 min. For PC treated samples (Fig. 5a), four intermediates (A1, A2, A8 and A9) more hydrophilic than A were detected at t_R = 2.6, 3.4, 3.2 and 3.9 min, respectively. Among them, A1 and A2 are the two major ones due to their high concentrations in the reaction mixtures. A3–A7 were the five detected intermediates more hydrophobic than that of l A. In teams of the concentration level in the reaction mixture, A3 is a major intermediate and its concentration was insensitive to the treatment time, and A4–A7 can be categorized as major intermediates. A4 was first determined from the sample at PC 300 s treatment and a similar concentration was also determined at 600 s. However, A4 concentration at 1200 s PC treated sample was below the detection limit, while a new hydrophobic intermediate, A5, was detected as a major intermediate at t_R = 6.7 min. A5 was undetectable in the reaction mixture of 2400 s PC treatment with the formation of a new major hydrophobic intermediate, A6 (t_R = 6.4 min). Interestingly, for 3000 s PC treatment, A6 became undetectable while another new major hydrophobic intermediate, A7 (t_R = 6.0 min) was generated. More interestingly, hydrophobicity of A4–A7 was in an order of A4 > A5 > A6 > A7 with almost same retention time decrease of 0.35 min. Considering the production of a subsequent intermediate was always slightly more hydrophilic and with the disappearance of the previous one, therefore, there is a possibility that these set of intermediates are the consecutive oxidation products of A4.

The obvious differences are easily identifiable by comparing the results obtained from PC treated A (a double-ringed purine base) samples (Fig. 5a) with the results obtained from PC treated U, C and T (single-ringed pyrimidine bases) samples (Figs. 4a, S3a and S4a). For all pyrimidine investigated, the degradation products are dominated by the intermediates more hydrophilic than their original molecules. For PC treated U and C samples, three detected hydrophobic intermediates were minor in terms of concentrations in reaction mixtures (Figs. 4a and S3a), while for PC treated T samples, no intermediates more hydrophobic than their original molecules were detected (Fig. S4a). This is in strong contrast to PC treated double-ringed purine base like A, where the hydrophilic intermediates are no longer the sole dominant products as the hydrophobic intermediates are also major intermediates in the reaction mixtures (Fig. 5a).

For PEC treated A samples (Fig. 5b), A1 was the dominant intermediate throughout the treatment process, though its concentration decreased slightly as the treatment time increased. A group of minor hydrophilic intermediates (A9, A10 and A12) were also recorded. However, only one hydrophobic intermediate (A11, t_R = 5.8 min) was detected from the PEC treated samples in comparison to four hydrophobic intermediates detected from PC treated samples. The results shown in Fig. 5b indicate that the intermediates that are more hydrophilic than its original molecule were the dominant products in PEC treated A samples. This is in strong contrast to the cases of PEC treated single-ringed pyrimidine bases, where the PEC degradation products in the reaction mixtures were dominated by the intermediates that are more hydrophobic than their original molecules (Figs. 4b, S3b and S4b).

3.4. Mechanistic considerations

The experimental results shown in Sections 3.1 and 3.2 clearly demonstrated the oxidative degradation behavior (in teams of degradation efficiency and kinetics) differences among single-ringed pyrimidine and double-ringed purine. These results also demonstrated the oxidative degradation behavior differences between PC and PEC processes. The experimental results presented in the section 3.4 revealed the oxidative degradation behavior differences of the nucleotide bases in teams of produced intermediates, which may be summarized as: (i) For a given nucleotide base, the intermediates produced by PC and PEC treatments are different in terms of hydrophilicity; (ii) for a given treatment method, the hydrophilicity characteristics of the intermediates are highly

Please cite this article in press as: G. Li, et al., Photocatalytic and photoelectrocatalytic degradation of small biological compounds at TiO_2 photoanode: A case study of nucleotide bases, Catal. Today (2014), http://dx.doi.org/10.1016/j.cattod.2014.04.029

dependent on the type of nucleotide bases involved. The single-ringed pyrimidine and the double-ringed purine belong to different categories.

Theoretically calculated $2FED_{HOMO}{}^2$ and $FED_{HOMO}{}^2 + FED_{LUMO}{}^2$ values (Table 2) indicated that for a given nucleotide base, the initial reaction sites are different for direct h^+ attack (in PEC process) and •OH attack (in PC process). These predictions agreed well with the experimental results presented above where for a given nucleotide base, PC and PEC differed remarkably from each other in terms of degradation efficiency and degradation intermediates. For a given treatment method (i.e., PC or PEC), the theoretically calculated $2FED_{HOMO}{}^2$ and $FED_{HOMO}{}^2 + FED_{LUMO}{}^2$ values of different nucleotide bases revealed that the initial reaction sites were depend on the type of nucleotide bases. For single-ringed pyrimidine like U, C and T, the initial reaction sites are likely to occur on the atoms within the 6-membered ring structure, regardless of treatment process. For double-ringed purine base such A, the initial reaction sites are likely to occur at the side-chain atoms of the 6-membered ring structure (PEC process) or on the 5-membered ring structure (PC process). These predictions again agreed well with the above experimental results where for a given treatment method, the single-ringed pyrimidine exhibited very different PC degradation behaviors in comparison to the double-ringed purine in terms of both degradation efficiency and hydrophilicity characteristics of intermediates.

The theoretical and experimental results obtained here suggested that the mechanistic pathway for PC and PEC processes differed from each other. The differences in PC degradation behaviors and products can be attributed to the different mechanistic pathways of PC and PEC processes. As aforementioned, according to reaction mechanisms reported to date, the photocatalytically and photoelectrocatalytically produced intermediates should be exclusively more hydrophilic than its original nucleotide base. However, the intermediates more hydrophobic than their original nucleotide bases were obtained in this study from both PC and PEC treated samples. This implies that the reported reaction mechanisms need to be further examined and validated. For this purpose, the chemical structures of the produced intermediates must be precisely identified. A systematic experimental work is currently under investigation to achieve this, and the findings will be reported in the near future.

4. Conclusions

In this work, the PC and PEC degradation of different nucleotide bases were comparatively investigated. A number of conclusions can be drawn based on the obtained results:

(1) For a given nucleotide base, PEC method possesses higher degradation efficiency than that of PC method; the superiority of PEC method over PC method becomes more obvious at higher concentrations of nucleotide base; for a given method, degradation efficiency is dependent on the type of nucleotide bases. Similar degradation behaviors were observed from all single-ringed pyrimidine investigated, which are distinctively different to that of the double-ringed purine.
(2) For a given nucleotide base, the hydrophilicity characteristics of PC produced intermediates are differed significantly from those of PEC produced intermediates; For a given method, similar hydrophilicity characteristics were obtained from all single-ringed pyrimidine investigated that differ significantly from those observed from the double-ringed purine.
(3) For a given nucleotide base, the theoretically calculated $2FED_{HOMO}{}^2$ and $FED_{HOMO}{}^2 + FED_{LUMO}{}^2$ values suggest that the initial reaction sites are different for PC and PEC processes, which agreed well with the experimental results; For a given method, the calculated values of different nucleotide bases suggest that the initial reaction sites for all single-ringed pyrimidine are likely to occur on the atoms within the 6-membered ring structure, while for double-ringed purine the initial reaction sites are likely to occur at side-chain atoms of the 6-membered ring structure (PEC process) or on 5-membered ring structure (PC process).
(4) Both theoretical calculation and experimental results suggest that the mechanistic pathway of PEC process differs from that of PC process.

Acknowledgments

This is contribution No. IS-1874 from GIGCAS. Authors thank Australian Research Council, NSFC (41373103 and 21077104) and The Science and Technology Project of Guangdong Province, China (2012A032300010).

Appendix A. Supplementary data

Supplementary data associated with this article can be found, in the online version, at http://dx.doi.org/10.1016/j.cattod.2014.04.029.

References

[1] D.L. Jiang, S.Q. Zhang, H.J. Zhao, Environ. Sci. Technol. 41 (2007) 303–308.
[2] H.J. Zhao, D.L. Jiang, S.Q. Zhang, W. Wen, J. Catal. 250 (2007) 102–109.
[3] G.Y. Li, Y.L. Zhang, H.W. Sun, J.B. An, X. Nie, H.J. Zhao, P.K. Wong, T.C. An, Catal. Today 201 (2013) 167–174.
[4] H.S. Fang, Y.P. Gao, G.Y. Li, J.B. An, P.K. Wong, H.Y. Fu, S.D. Yao, X.P. Nie, T.C. An, Environ. Sci. Technol. 47 (2013) 2704–2712.
[5] Z. Topalian, B.I. Stefanov, C.G. Granqvist, L. Osterlund, J. Catal. 307 (2013) 265–274.
[6] D.Q. Zhang, G.S. Li, J.C. Yu, J. Mater. Chem. 20 (2010) 4529–4536.
[7] A. Turki, H. Kochkar, I. Garcia-Fernandez, M.I. Polo-Lopez, A. Ghorbel, C. Guillard, G. Berhault, P. Fernandez-Ibanez, Catal. Today 209 (2013) 147–152.
[8] N. Yamada, M. Suzumura, F. Koiwa, N. Negishi, Water Res. 47 (2013) 2770–2776.
[9] G. Vereb, L. Manczinger, G. Bozso, A. Sienkiewicz, L. Forro, K. Mogyorosi, K. Hernadi, A. Dombi, Appl. Catal. B: Environ. 129 (2013) 566–574.
[10] K. Pathakoti, S. Morrow, C. Han, M. Pelaez, X. He, D.D. Dionysiou, H.M. Hwang, Environ. Sci. Technol. 47 (2013) 9988–9996.
[11] X.P. Wang, Y.X. Tang, Z. Chen, T.T. Lim, J. Mater. Chem. 22 (2012) 23149–23158.
[12] H. Hidaka, S. Horikoshi, N. Serpone, J. Knowland, J. Photochem. Photobiol. A 111 (1997) 205–213.
[13] P.F. Biard, A. Bouzaza, D. Wolbert, Environ. Sci. Technol. 41 (2007) 2908–2914.
[14] S. Horikoshi, N. Serpone, S. Yoshizawa, J. Knowland, H. Hidaka, J. Photochem. Photobiol. A 120 (1999) 63–74.
[15] J. Cadet, J.R. Wagner, Csh. Perspect. Biol. 5 (2013).
[16] G.M. Rodríguez-Muñiz, M.L. Marin, V. Lhiaubet-Vallet, M.A. Miranda, Chem. Eur. J. 18 (2012) 8024–8027.
[17] H.K. Singh, M. Saquib, M.M. Haque, M. Muneer, J. Hazard. Mater. 142 (2007) 425–430.
[18] C. Jaussaud, O. Paisse, R. Faure, J. Photochem. Photobiol. A 130 (2000) 157–162.
[19] S. Saltzman, A.J. Acher, N. Brates, M. Horowitz, A. Gevelberg, Pesticide Sci. 13 (1982) 211–217.
[20] A.F. Pozharskii, A.T. Soldatenkov, A.R. Katritzky, Heterocycles in Life and Society: An Introduction to Heterocyclic Chemistry and Biochemistry and the Role of Heterocycles in Science, Technology, Medicine, and Agriculture, John Wiley and Sons, New York, 1997.
[21] M.R. Dhananjeyan, R. Annapoorani, R. Renganathan, J. Photochem. Photobiol. A 109 (1997) 147–153.
[22] W. Bahnemann, M. Muneer, M.M. Haque, Catal. Today 124 (2007) 133–148.
[23] H. Hidaka, E. Garcia-Lopez, L. Palmisano, N. Serpone, Appl. Catal. B: Environ. 78 (2008) 139–150.
[24] S. Horikoshi, H. Hidaka, J. Photochem. Photobiol. A 141 (2001) 201–207.
[25] M. Carrier, C. Guillard, M. Besson, C. Bordes, H. Chermette, J. Phys. Chem. A 113 (2009) 6365–6374.
[26] P. Calza, E. Pelizzetti, C. Minero, J. Appl. Electrochem. 35 (2005) 665–673.
[27] V. Maurino, C. Minero, E. Pelizzetti, P. Piccinini, N. Serpone, H. Hidaka, J. Photochem. Photobiol. A 109 (1997) 171–176.
[28] K. Nohara, H. Hidaka, E. Pelizzetti, N. Serpone, Catal. Lett. 36 (1996) 115–118.
[29] R. Cathcart, E. Schwiers, R.L. Saul, B.N. Ames, Proc. Natl. Acad. Sci. U. S. A. – Biol. 81 (1984) 5633–5637.

[30] M.R. Dhananjeyan, R. Annapoorani, S. Lakshmi, R. Renganathan, J. Photochem. Photobiol. A 96 (1996) 187–191.
[31] K. Vinodgopal, S. Hotchandani, P.V. Kamat, J. Phys. Chem. – US 97 (1993) 9040–9044.
[32] P.A. Mandelbaum, A.E. Regazzoni, M.A. Blesa, S.A. Bilmes, J. Phys. Chem. B 103 (1999) 5505–5511.
[33] D.L. Jiang, H.J. Zhao, S.Q. Zhang, R. John, J. Phys. Chem. B 107 (2003) 12774–12780.
[34] H.J. Zhao, D.L. Jiang, S.Q. Zhang, K. Catterall, R. John, Anal. Chem. 76 (2004) 155–160.
[35] M.R. Hoffmann, S.T. Martin, W.Y. Choi, D.W. Bahnemann, Chem. Rev. 95 (1995) 69–96.
[36] D.L. Jiang, H.J. Zhao, S.Q. Zhang, R. John, J. Photochem. Photobiol. A 177 (2006) 253–260.
[37] D.L. Jiang, H.J. Zhao, S.Q. Zhang, R. John, G.D. Will, J. Photochem. Photobiol. A 156 (2003) 201–206.
[38] Y. Ohko, K.I. Iuchi, C. Niwa, T. Tatsuma, T. Nakashima, T. Iguchi, Y. Kubota, A. Fujishima, Environ. Sci. Technol. 36 (2002) 4175–4181.
[39] X. Zhang, F. Wu, X.W. Wu, P.Y. Chen, N.S. Deng, J. Hazard. Mater. 157 (2008) 300–307.
[40] G.Y. Li, X.L. Liu, H.M. Zhang, T.C. An, S.Q. Zhang, A.R. Carroll, H.J. Zhao, J. Catal. 277 (2011) 88–94.
[41] G.Y. Li, X.L. Liu, H.M. Zhang, P.K. Wong, T.C. An, H.J. Zhao, Appl. Catal. B: Environ. 140–141 (2013) 225–232.
[42] S.Q. Zhang, D.L. Jiang, H.J. Zhao, Environ. Sci. Technol. 40 (2006) 2363–2368.
[43] E. Pelizzetti, P. Calza, G. Mariella, V. Maurino, C. Minero, H. Hidaka, Chem. Commun. (2004) 1504–1505.

Please cite this article in press as: G. Li, et al., Photocatalytic and photoelectrocatalytic degradation of small biological compounds at TiO_2 photoanode: A case study of nucleotide bases, Catal. Today (2014), http://dx.doi.org/10.1016/j.cattod.2014.04.029